Chiral Phosphoric Acid Catalysis: The Terada Model Revisited

Matthew N. Grayson*

Department of Chemistry, University of Bath, Claverton Down, Bath BA2 7AY, UK

TOC graphic

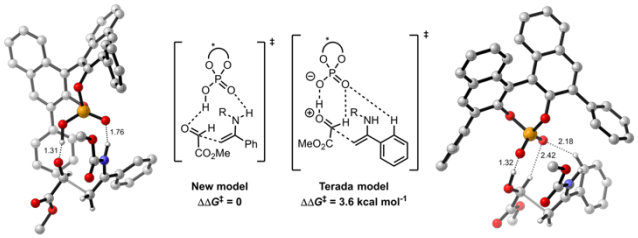

ABSTRACT:

Since Akiyama and Terada independently reported the introduction of chiral phosphoric acids (CPAs) as effective catalysts for Mannich-type reactions in 2004, the field of CPA catalysis has grown immensely. Terada reported in 2008 the first example of the activation of aldehydes by a CPA. Based on density functional theory (DFT) calculations, Terada proposed a dual activation mode for this enantioselective aza-ene-type reaction between an aldehyde and an enecarbamate. In this model, hydrogen bonds between the catalyst's hydroxyl group and the carbonyl oxygen and the catalyst's P=O and the formyl proton were observed; the nucleophile then attacks without coordination to the catalyst. This reaction model provided the mechanistic basis for understanding Terada's reaction and many other asymmetric transformations since. In the present study, DFT calculations are reported that identify a lower energy mechanism for this landmark reaction. In this new model, hydrogen bonds between the catalyst's hydroxyl group and the aldehyde oxygen and the catalyst's P=O and the NH group of the enecarbamate are seen. The new model rationalizes the stereoselective outcome of Terada's reaction and offers insight into why a more sterically demanding catalyst gives lower levels of enantioselectivity.

INTRODUCTION

In 2004, Akiyama[1] and Terada[2] independently reported the introduction of chiral phosphoric acids (CPAs) as effective catalysts for Mannich-type reactions. Since then, CPAs have been found to catalyze a wide range of asymmetric reactions and have been used extensively in the synthesis of biologically active natural products.[3–6]

The first example of the activation of aldehydes by a CPA was the enantioselective aza-ene-type reaction between an aldehyde and an enecarbamate reported by Terada in 2008 (Scheme 1).[7] In this landmark study, the preferred activation mode was identified through density functional theory (DFT) calculations. Although no transition state structures (TSs) were located, hydrogen bonds between the catalyst's hydroxyl group and the carbonyl oxygen and the catalyst's P=O and the formyl proton were observed in the lowest energy complex between CPA and aldehyde. These interactions were supported by X-ray crystallographic analysis of complexes between carboxylic acids and dimethylformamide.[8,9] It was proposed that the enecarbamate then attacks from the least hindered face of the aldehyde without coordination to the catalyst (Terada model, Scheme 1). This dual activation mode has been widely adopted and has provided the basis for many proposed mechanisms in CPA catalysis.[10] Examples include the CPA-catalyzed hetero-Diels−Alder,[11] aldol-type,[12,13] allenylboration[14] and multicomponent coupling[15] reactions. It has also influenced computational work on related CPA-catalyzed reactions including work by Goodman[16,17] and Houk[18–21]. However, an alternative bifunctional activation mode was not considered in Terada's original work.

In the present study, DFT calculations have identified a new mechanism that is lower in energy than Terada's model in which the CPA coordinates to both the nucleophile and the electrophile (New model, Scheme 1). In this bifunctional activation mode, hydrogen bonds are seen between the catalyst's hydroxyl group and the aldehyde oxygen and the catalyst's P=O and the NH group of the enecarbamate. The new model also rationalizes the stereoselective outcome of Terada's reaction.

Scheme 1 Terada's phosphoric acid-catalyzed asymmetric aza-ene-type reaction and possible activation modes.

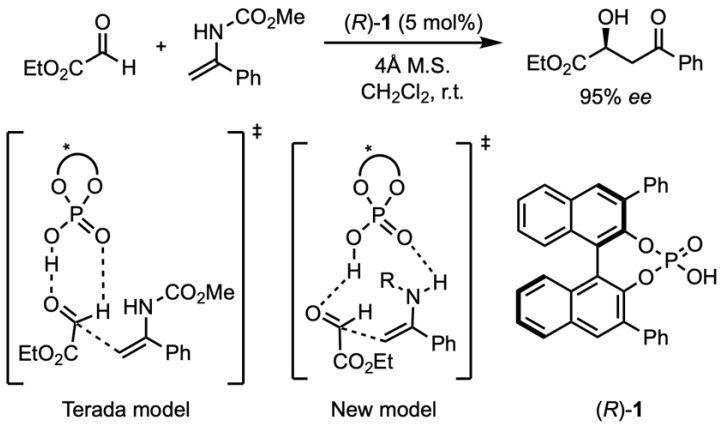

RESULTS AND DISCUSSION

To explore the preferred activation mode of Terada's phosphoric acid-catalyzed asymmetric aza-ene-type reaction, C−C bond forming TSs were located at the B3LYP-D3(BJ)/def2-TZVPP−IEF-PCM(dichloromethane)//B3LYP/6-31G(d) level of theory[22–26] using Gaussian 16[27] (see Supporting Information for full computational details). The ethyl ester of the electrophile was replaced by a methyl ester to reduce conformational flexibility and thus simplify the calculations. This truncation was shown to have minimal effect on the calculated TSs (see Supporting Information, Figure S1). The lowest energy TS was **TS-1*Si*** (Figure 1) which corresponds to the new bifunctional activation mode proposed in Scheme 1 and leads to the major product observed experimentally. The lowest energy Terada-like TS (**TS-2*Si***) was calculated to be disfavored by 3.6 kcal mol^{-1} relative to **TS-1*Si*** due to the absence of the strong N-H···O interaction. Although the catalyst-electrophile interactions seen in **TS-2*Si*** correspond to those proposed in Terada's dual activation mode, a C-H···O interaction is present between catalyst and nucleophile. The lowest energy TS that has interactions between catalyst and electrophile only (Terada model from Figure 1 but lacking the additional aryl P=O···H-C interaction) was calculated to be 5.4 kcal mol^{-1} higher in energy than **TS-1*Si***. A third, low energy activation mode was identified in which hydrogen bonds are seen between the catalyst's hydroxyl group and the aldehyde oxygen and the catalyst's P=O and a vinylic proton of the enecarbamate (**TS-3*Si***). **TS-3*Si*** was calculated to be lower in energy than **TS-2*Si*** but disfavored by 3.4 kcal mol^{-1} relative to **TS-1*Si***.

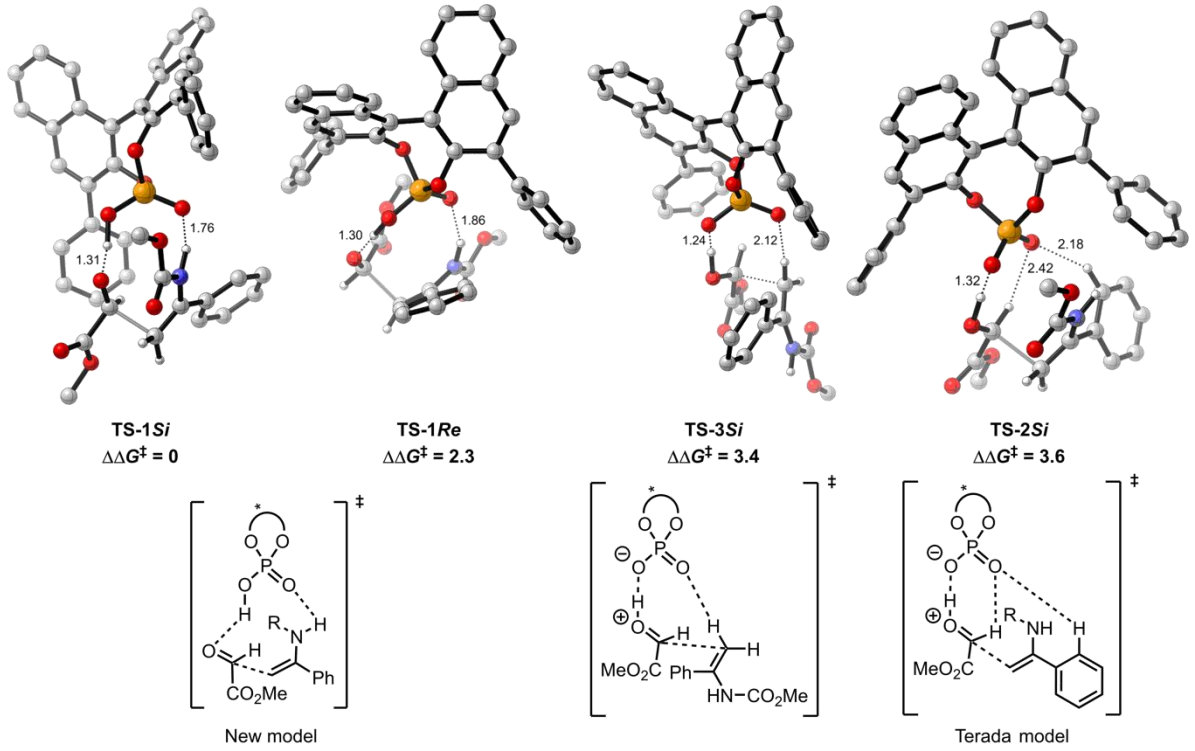

Figure 1. Comparison of activation modes in the (*R*)-**1**-catalyzed asymmetric aza-ene-type reaction. TSs are numbered according to when they are first discussed in the text. Non-critical hydrogen atoms omitted for clarity. All energies in kcal mol^{-1}.

By taking a Boltzmann distribution of all TS conformations within 3 kcal mol^{-1} of **TS-1*Si***, an ee value of 95% at 298.15 K was computed which is in full agreement with the experimental data. **TS-1*Re***, the lowest energy TS leading to the minor enantiomer of the product, was calculated to be disfavored by 2.3 kcal mol^{-1} relative to **TS-1*Si*** (Figure 1). To understand the origin of this energy difference, the CPA was optimized in isolation. The lowest energy catalyst conformation is shown in Figure 2 alongside **TS-1*Re*** and **TS-1*Si***. In **TS-1*Si***, the dihedral angle highlighted in green is close to the angle adopted in the isolated catalyst but in **TS-1*Re***, this angle is distorted away from its ideal value. The steric bulk of the aldehyde is placed underneath the catalyst in **TS-1*Re*** and so a larger dihedral angle avoids a steric clash between aldehyde and catalyst. This is supported by a larger catalyst distortion energy in **TS-1*Re*** relative to **TS-1*Si*** (see Table S1 in Supporting Information). Torsional effects also contribute to the difference in energy between **TS-1*Re*** and **TS-1*Si***. In **TS-1*Si***, the bulky groups of the nucleophile and electrophile approach anti to each other. In **TS-1*Re***, this approach is gauche. This insight is supported by a larger substrate pair distortion energy in **TS-1*Re*** relative to **TS-1*Si*** (see Table S1 in Supporting Information). The new model also accounts for the high levels of

diastereoselectivity observed for substituted enecarbamates (see Page S6 of Supporting Information).

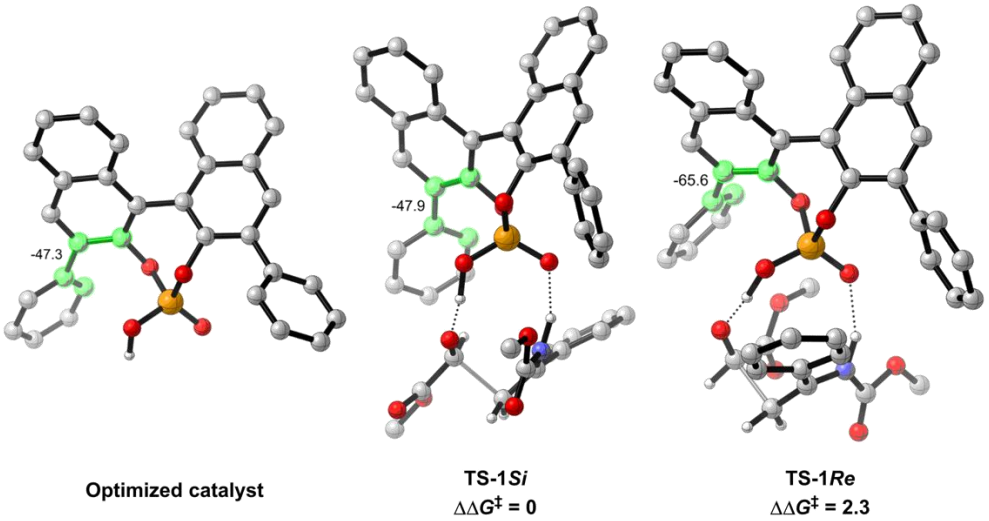

Figure 2. Comparison of catalyst structure in the C-C bond forming TSs in the (*R*)-**1**-catalyzed asymmetric aza-ene-type reaction. Non-critical hydrogen atoms omitted for clarity. All energies in kcal mol^{-1}.

In phosphoric acid catalysis, more sterically demanding 3 and 3′ groups generally lead to higher levels of enantioselectivity.[28] In the phosphoric acid-catalyzed asymmetric aza-ene-type reaction however, this is not the case and enantioselectivity drops significantly when (*R*)-**2** is employed instead of (*R*)-**1** (Figure 3). To explain this observation, TSs were located for the reaction catalyzed by (*R*)-**2** (see Supporting Information). **TS-4*Si*** and **TS-4*Re*** were calculated to be the lowest energy diastereomeric TSs and are similar in geometry to **TS-1*Si*** and **TS-1*Re*** but are much closer in free energy (Figure 3). In **TS-4*Re***, stabilizing CH···π interactions are observed between the substrate and the 3 and 3′ groups; such interactions are not seen to the less electron-rich aromatic groups present in **TS-1*Re***. These interactions stabilize **TS-4*Re*** relative to **TS-4*Si*** and thus account for the lower levels of enantioselectivity observed experimentally with (*R*)-**2**.

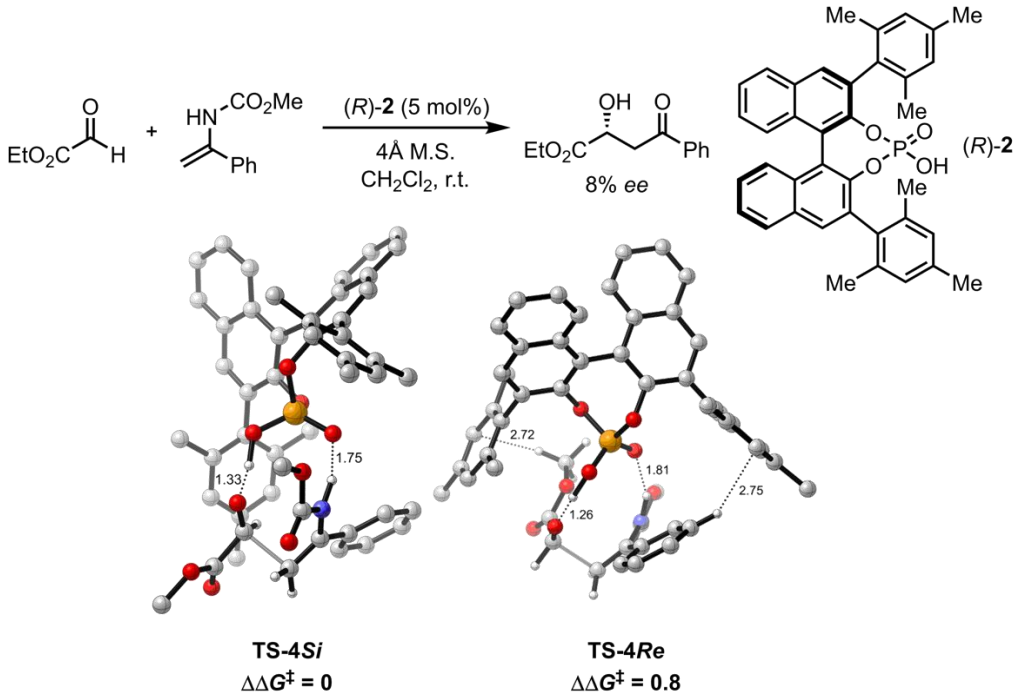

Figure 3. C-C bond forming TSs for the (*R*)-**2**-catalyzed asymmetric aza-ene-type reaction. Non-critical hydrogen atoms omitted for clarity. All energies in kcal mol^{-1}.

CONCLUSIONS

In summary, a new model for the phosphoric acid-catalyzed asymmetric aza-ene-type reaction has been proposed. In this bifunctional activation mode, hydrogen bonds between the catalyst's hydroxyl group and the aldehyde oxygen and the catalyst's P=O and the NH group of the enecarbamate are seen. DFT calculations show that the new model is lower in energy than Terada's dual activation model in which hydrogen bonds between the catalyst's hydroxyl group and the carbonyl oxygen and the catalyst's P=O and the formyl proton were observed. The stereoselective outcome of the aza-ene-type reaction is rationalized through catalyst and substrate distortion present in the TS leading to the minor product. Lower levels of enantioselectivity seen in the presence of a more sterically demanding catalyst are rationalized through stabilizing CH···π interactions identified in the TS leading to the minor product. It is hoped that this new insight into phosphoric acid catalysis will enable further development of synthetic methodology involving these important catalysts.

ASSOCIATED CONTENT

Supporting Information. Full details of computational methods used, complete list of energies, frequencies and molecular geometries (Cartesian coordinates) for all computed structures. All Cartesian coordinates were generated by the ESIgen software.[29]

The Supporting Information is available free of charge on the ACS Publications website.

AUTHOR INFORMATION

Corresponding Author

*M.N.Grayson@bath.ac.uk

Notes

The author declares no competing financial interest.

ACKNOWLEDGMENT

M.N.G. thanks the University of Bath for financial support. This research made use of the Balena High Performance Computing (HPC) Service at the University of Bath.

REFERENCES

(1) Akiyama, T.; Itoh, J.; Yokota, K.; Fuchibe, K. Enantioselective Mannich-Type Reaction Catalyzed by a Chiral Brønsted Acid. *Angew. Chemie Int. Ed.* **2004**, *43* (12), 1566–1568.

(2) Uraguchi, D.; Terada, M. Chiral Brønsted Acid-Catalyzed Direct Mannich Reactions via Electrophilic Activation. *J. Am. Chem. Soc.* **2004**, *126* (17), 5356–5357.

(3) Akiyama, T. Stronger Brønsted Acids. *Chem. Rev.* **2007**, *107* (12), 5744–5758.

(4) Terada, M. Chiral Phosphoric Acids as Versatile Catalysts for Enantioselective Transformations. *Synthesis* **2010**, *2010* (12), 1929–1982.

(5) Parmar, D.; Sugiono, E.; Raja, S.; Rueping, M. Complete Field Guide to Asymmetric BINOL-Phosphate Derived Brønsted Acid and Metal Catalysis: History and Classification by Mode of Activation; Brønsted Acidity, Hydrogen Bonding, Ion Pairing, and Metal Phosphates. *Chem. Rev.* **2014**, *114* (18), 9047–9153.

(6) Sedgwick, D. M.; Grayson, M. N.; Fustero, S.; Barrio, P. Recent Developments and Applications of the Chiral Bronsted Acid Catalyzed Allylboration of Carbonyl Compounds. *Synthesis* **2018**, *50* (10), 1935–1957.

(7) Terada, M.; Soga, K.; Momiyama, N. Enantioselective Activation of Aldehydes by Chiral Phosphoric Acid Catalysts in an Aza-Ene-Type Reaction between Glyoxylate

and Enecarbamate. *Angew. Chem. Int. Ed.* **2008**, *47* (22), 4122–4125.

(8) Czugler, M.; Stezowski, J. J.; Weber, E. Co-Ordination-Assisted Inclusion of Neutral Molecules by the Racemic 9,9′-Spirobifluorene-2,2′-Dicarboxylic Acid Host Lattice. X-Ray Crystal Structure of the Dimethylformamide Clathrate at 170 K. *J. Chem. Soc., Chem. Commun.* **1983**, No. 4, 154–155.

(9) Csöregh, I.; Sjögren, A.; Czugler, M.; Cserzö, M.; Weber, E. Versatility of the 1,1′-Binaphthyl-2,2′-Dicarboxylic Acid Host in Solid-State Inclusion: Crystal and Molecular Structures of the Dimethylformamide (1 : 2), Dimethyl Sulphoxide (1 : 1), and Bromobenzene (1 : 1) Clathrates. *J. Chem. Soc., Perkin Trans. 2* **1986**, No. 4, 507–513.

(10) Rueping, M.; Kuenkel, A.; Atodiresei, I. Chiral Brønsted Acids in Enantioselective Carbonyl Activations - Activation Modes and Applications. *Chem. Soc. Rev.* **2011**, *40* (9), 4539–4549.

(11) Momiyama, N.; Tabuse, H.; Terada, M. Chiral Phosphoric Acid-Governed Anti-Diastereoselective and Enantioselective Hetero-Diels−Alder Reaction of Glyoxylate. *J. Am. Chem. Soc.* **2009**, *131* (36), 12882–12883.

(12) Terada, M.; Tanaka, H.; Sorimachi, K. Enantioselective Direct Aldol-Type Reaction of Azlactone via Protonation of Vinyl Ethers by a Chiral Brønsted Acid Catalyst. *J. Am. Chem. Soc.* **2009**, *131* (10), 3430–3431.

(13) Ren, L.; Lian, X.-L.; Gong, L.-Z. Brønsted Acid/Rhodium(II) Cooperative Catalytic Asymmetric Three-Component Aldol-Type Reaction for the Synthesis of 3-Amino Oxindoles. *Chem. - Eur. J.* **2013**, *19* (10), 3315–3318.

(14) Reddy, L. R. Chiral Brønsted Acid Catalyzed Enantioselective Propargylation of Aldehydes with Allenylboronate. *Org. Lett.* **2012**, *14* (4), 1142–1145.

(15) Cala, L.; Mendoza, A.; Fañanás, F. J.; Rodríguez, F. A Catalytic Multicomponent Coupling Reaction for the Enantioselective Synthesis of Spiroacetals. *Chem. Commun.* **2013**, *49* (26), 2715–2717.

(16) Grayson, M. N.; Pellegrinet, S. C.; Goodman, J. M. Mechanistic Insights into the BINOL-Derived Phosphoric Acid-Catalyzed Asymmetric Allylboration of Aldehydes. *J. Am. Chem. Soc.* **2012**, *134* (5), 2716–2722.

(17) Grayson, M. N.; Goodman, J. M. Understanding the Mechanism of the Asymmetric Propargylation of Aldehydes Promoted by 1,1'-Bi-2-Naphthol-Derived Catalysts. *J. Am. Chem. Soc.* **2013**, *135* (16), 6142–6148.

(18) Wang, H.; Jain, P.; Antilla, J. C.; Houk, K. N. Origins of Stereoselectivities in Chiral

Phosphoric Acid Catalyzed Allylborations and Propargylations of Aldehydes. *J. Org. Chem.* **2013**, *78* (3), 1208–1215.

(19) Grayson, M. N.; Krische, M. J.; Houk, K. N. Ruthenium-Catalyzed Asymmetric Hydrohydroxyalkylation of Butadiene: The Role of the Formyl Hydrogen Bond in Stereochemical Control. *J. Am. Chem. Soc.* **2015**, *137* (27), 8838–8850.

(20) Rodríguez, E.; Grayson, M. N.; Asensio, A.; Barrio, P.; Houk, K. N.; Fustero, S. Chiral Brønsted Acid-Catalyzed Asymmetric Allyl(Propargyl)Boration Reaction of *Ortho* -Alkynyl Benzaldehydes: Synthetic Applications and Factors Governing the Enantioselectivity. *ACS Catal.* **2016**, *6* (4), 2506–2514.

(21) Grayson, M. N.; Yang, Z.; Houk, K. N. Chronology of CH···O Hydrogen Bonding from Molecular Dynamics Studies of the Phosphoric Acid-Catalyzed Allylboration of Benzaldehyde. *J. Am. Chem. Soc.* **2017**, *139* (23), 7717–7720.

(22) Simón, L.; Goodman, J. M. How Reliable Are DFT Transition Structures? Comparison of GGA, Hybrid-Meta-GGA and Meta-GGA Functionals. *Org. Biomol. Chem.* **2011**, *9* (3), 689–700.

(23) Jindal, G.; Sunoj, R. B. Axially Chiral Imidodiphosphoric Acid Catalyst for Asymmetric Sulfoxidation Reaction: Insights on Asymmetric Induction. *Angew. Chemie Int. Ed.* **2014**, *53* (17), 4432–4436.

(24) Lam, Y. -h.; Houk, K. N. How Cinchona Alkaloid-Derived Primary Amines Control Asymmetric Electrophilic Fluorination of Cyclic Ketones. *J. Am. Chem. Soc.* **2014**, *136* (27), 9556–9559.

(25) Lam, Y. -h.; Houk, K. N. Origins of Stereoselectivity in Intramolecular Aldol Reactions Catalyzed by Cinchona Amines. *J. Am. Chem. Soc.* **2015**, *137* (5), 2116–2127.

(26) Champagne, P. A.; Houk, K. N. Origins of Selectivity and General Model for Chiral Phosphoric Acid-Catalyzed Oxetane Desymmetrizations. *J. Am. Chem. Soc.* **2016**, *138* (38), 12356–12359.

(27) Frisch, M. J.; Trucks, G. W.; Schlegel, H. B.; Scuseria, G. E.; Robb, M. A.; Cheeseman, J. R.; Scalmani, G.; Barone, V.; Mennucci, B.; Petersson, G. A.; Nakatsuji, H.; Caricato, M.; Li, X.; Hratchian, H. P.; Izmaylov, A. F.; Bloino, J.; Zheng, J.; Sonnenberg, J. L.; Hada, M.; Ehara, M.; Toyota, K.; Fukuda, R.; Hasegawa, J.; Ishida, M.; Nakajima, T.; Honda, Y.; Kitao, O.; Nakai, H.; Vreven, T.; Montgomery, J. A.; Peralta, J. E.; Ogliaro, F.; Bearpark, M.; Heyd, J. J.; Brothers, E.; Kudin, K. N.; Staroverov, V. N.; Kobayashi, R.; Normand, J.; Raghavachari, K.; A.

Rendell, J. C.; Burant, S.; Iyengar, S.; Tomasi, J.; Cossi, M.; Rega, N.; Millam, J. M.; Klene, M.; Knox, J. E.; Cross, J. B.; Bakken, V.; Adamo, C.; Jaramillo, J.; Gomperts, R.; Stratmann, R. E.; Yazyev, O.; Austin, A. J.; Cammi, R.; Pomelli, C.; Ochterski, J. W.; Martin, R. L.; Morokuma, K.; Zakrzewski, V. G.; Voth, G. A.; Salvador, P.; Dannenberg, J. J.; Dapprich, S.; Daniels, A. D.; Farkas, O.; Foresman, J. B.; Ortiz, J. V.; Cioslowski, J.; Fox, D. J. *Gaussian 16*, Revision A.03; Gaussian, Inc.: Wallingford CT, 2016.

(28) Reid, J. P.; Simón, L.; Goodman, J. M. A Practical Guide for Predicting the Stereochemistry of Bifunctional Phosphoric Acid Catalyzed Reactions of Imines. *Acc. Chem. Res.* **2016**, *49* (5), 1029–1041.

(29) Pedregal, J. R.-G.; Gómez-Orellana, P.; Maréchal, J.-D. ESIgen: Electronic Supporting Information Generator for Computational Chemistry Publications. *J. Chem. Inf. Model.* **2018**, *58* (3), 561–564.